Excitation of multiple surface-plasmon-polariton waves guided by the periodically corrugated interface of a metal and a periodic multilayered isotropic dielectric material

Muhammad Faryad,[1] Anthony Shoji Hall,[2] Greg D. Barber,[2,3] Thomas E. Mallouk,[2,3] and Akhlesh Lakhtakia[1,3,*]

[1]*Nanoengineered Metamaterials Group, Department of Engineering Science and Mechanics, Pennsylvania State University, University Park, Pennsylvania 16802, USA*
[2]*Department of Chemistry, Pennsylvania State University, University Park, Pennsylvania 16802, USA*
[3]*Materials Research Institute, Pennsylvania State University, University Park, Pennsylvania 16802, USA*
**Corresponding author: akhlesh@psu.edu*

Received December 21, 2011; revised January 22, 2012; accepted January 23, 2012; posted January 24, 2012 (Doc. ID 160421); published March 20, 2012

The excitation of multiple surface-plasmon-polariton (SPP) waves guided by the periodically corrugated interface of a homogeneous metal and a periodic multilayered isotropic dielectric (PMLID) material was studied theoretically. The solution of the underlying canonical boundary-value problem (with a planar interface) indicates that multiple SPP waves of different polarization states, phase speeds, and attenuation rates can be guided by the periodically corrugated interface. Accordingly, the boundary-value problem was formulated using rigorous coupled-wave analysis and solved using a numerically stable algorithm. A linearly polarized plane wave was considered obliquely incident on a PMLID material of finite thickness and backed by a metallic surface-relief grating. The total reflectance, total transmittance, and the absorptance were calculated as functions of the incidence angle for different numbers of unit cells in the PMLID material of fixed period. The excitation of SPP waves was indicated by those peaks in the absorptance curves that were independent of the number of unit cells, and these peaks were also correlated with the solutions of a dispersion equation obtained from the canonical boundary-value problem.

OCIS codes: 240.0310, 240.5420, 240.6680, 240.6690.

1. INTRODUCTION

In a seminal paper Yeh *et al.* [1] provided the general formulation for the propagation of electromagnetic surface waves guided by the planar interface of a homogeneous isotropic dielectric material and a periodic multilayered isotropic dielectric (PMLID) material. Since then, numerous theoretical and experimental investigations on the propagation and excitation of surface-plasmon-polariton (SPP) waves guided by the interface of a homogeneous metal and a PMLID material have been reported. In the vast majority, if not all of these papers, numerical results have been provided when the unit cell of the PMLID material consists of two different homogeneous dielectric layers, and it has been shown that p-polarized SPP waves can be guided by the chosen interface.

Some researchers [2–5] have shown experimentally and theoretically that s-polarized SPP waves can also be guided by such interfaces. Based on our recent theoretical investigations [6,7] on the guidance of multiple SPP waves at a certain frequency by the interface of a metal and a rugate filter—which is a continuously nonhomogeneous, not piecewise homogeneous, material [8,9]—we hypothesized that success or failure in finding s-polarized SPP waves could be attributed to the thickness of the first homogeneous dielectric layer in the unit cell adjacent to the metal. If that thickness is much greater than the penetration depth of the SPP wave into that layer, the effect of periodic nonhomogeneity of the PMLID material is going to be inconsequential. If that thickness is sufficiently small, then the periodic nonhomogeneity could be effective in the emergence of multiple SPP waves, some p and the others s polarized. Provided the thickness of the unit cell of the PMLID material remains unchanged, it would appear that the propensity to guide multiple SPP waves would be enhanced if the unit cell comprises several layers of comparable (but not large) thickness.

With a two-layer unit cell on the one hand, either sufficient to guide multiple SPP waves (including those of the s-polarization state) or not, and a unit cell with continuously varying relative permittivity on the other hand typically guiding several SPP waves, we decided to investigate an intermediate case where the number of layers in one unit cell exceeds two but is not so large that the PMLID material is, in effect, continuously nonhomogeneous. As the excitation of just a single SPP wave (at a given frequency) at the interface of a metal and a homogeneous semiconductor has recently been shown to improve the efficiency of thin-film solar cells [10,11], motivation for the work reported here came from the thought that the simultaneous excitation of several SPP waves—of different polarization states, phase speeds, e-folding distances along the direction of propagation, and field distributions, but all of the same frequency—would improve the efficiency even more. The piecewise homogeneous constitution of the PMLID material makes it attractive to fabricate even on an industrial scale.

Although the theoretical formulation for the underlying boundary-value problem has been provided by Yeh *et al.* [1], we have succinctly described it in 4×4 matrix notation in Subsection 2.A for completeness. For a practical implementation, we could have chosen either (i) the Turbadar–Kretschmann–Raether configuration [12–15], in which the interface of the metal and the dielectric material is planar but a prism is required to launch SPP waves [3–5,16], or (ii) the grating-coupled configuration in which the interface of the two partnering materials is periodically corrugated [17–19]. We chose the latter because it does not need a prism and it also allows the efficient coupling of SPP waves, which are otherwise nonradiative, with light. Furthermore, this configuration is of significance for thin-film solar cells with periodically nanopatterned back-surface reflectors [10,20,21]. Essential details are described in Subsection 2.B. Numerical results based on experimentally determined relative permittivities of the metal and the dielectric layers in the PMLID material are presented and discussed in Section 3. Concluding remarks are presented in Section 4.

An $\exp(-i\omega t)$ time dependence is implicit, with ω denoting the angular frequency. The free-space wavenumber, the free-space wavelength, and the phase speed in free space are denoted by $k_0=\omega\sqrt{\varepsilon_0\mu_0}$, $\lambda_0=2\pi/k_0$, and $c=1/\sqrt{\varepsilon_0\mu_0}$, respectively, with μ_0 and ε_0 being the permeability and permittivity of free space. Vectors are in boldface, column vectors are in boldface and enclosed within square brackets, and matrices are twice and square bracketed. The asterisk denotes the complex conjugate, and the Cartesian unit vectors are identified as $\hat{\mathbf{u}}_x$, $\hat{\mathbf{u}}_y$, and $\hat{\mathbf{u}}_z$.

2. THEORY IN BRIEF

A. Canonical Boundary-Value Problem: Planar Metal/PMLID Interface

Let the half-space $z\le0$ be occupied by an isotropic and homogeneous metal with complex-valued relative permittivity scalar ϵ_m. The region $z\ge0$ is occupied by a PMLID material with period 2Ω, as shown schematically in Fig. 1. The unit cell has N layers, the width and the relative permittivity of the jth layer, $j\in[1,N]$, being denoted by d_j and ϵ_{rj}, respectively; $\sum_{j=1}^{N} d_j=2\Omega$.

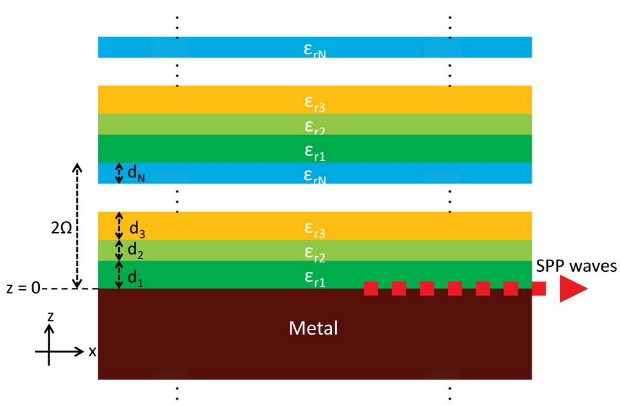

Fig. 1. (Color online) Schematic of the canonical boundary-value problem involving a planar interface between a homogeneous and isotropic metal and a periodic multilayered isotropic dielectric material.

Without any loss of generality, let an SPP wave propagate parallel to the unit vector $\hat{\mathbf{u}}_x$ guided by the interface $z=0$ and attenuate as $z\to\pm\infty$. Therefore, in the region $z\le0$, the wave vector may be written as

$$\mathbf{k}_{\mathrm{met}}=\kappa\hat{\mathbf{u}}_x-\alpha_{\mathrm{met}}\hat{\mathbf{u}}_z, \tag{1}$$

where $\kappa^2+\alpha_{\mathrm{met}}^2=k_0^2\epsilon_m$, κ is complex valued, and $\mathrm{Im}(\alpha_{\mathrm{met}})>0$ for attenuation as $z\to-\infty$. Accordingly, the electric field phasor in the metallic half-space may be written as

$$\mathbf{E}(\mathbf{r})=\left[a_p\left(\frac{\alpha_{\mathrm{met}}}{k_0}\hat{\mathbf{u}}_x+\frac{\kappa}{k_0}\hat{\mathbf{u}}_z\right)+a_s\hat{\mathbf{u}}_y\right]\exp(i\mathbf{k}_{\mathrm{met}}\cdot\mathbf{r}),\qquad z\le0, \tag{2}$$

and the magnetic field phasor may then be obtained by substitution of Eq. (2) in the Faraday equation. Here, a_p and a_s are unknown scalars with the same units as the electric field, and the subscripts p and s, respectively, denote the p- (parallel-) and s- (perpendicular-) polarization states with respect to the x–z plane.

For field representation in the half-space $z>0$, let us write $\mathbf{E}(\mathbf{r})=\mathbf{e}(z)\exp(i\kappa x)$ and $\mathbf{H}(\mathbf{r})=\mathbf{h}(z)\exp(i\kappa x)$. Substitution of the foregoing equations in the Faraday and the Ampére–Maxwell equations results in the matrix ordinary differential equation

$$\frac{d}{dz}[\mathbf{f}(z)]=i[\underline{\underline{P}}_j]\cdot[\mathbf{f}(z)],\qquad j\in[1,\infty), \tag{3}$$

for the jth layer in the PMLID material, where the column vector $[\mathbf{f}(z)]=[\,e_x(z)\quad e_y(z)\quad h_x(z)\quad h_y(z)\,]^T$ and the 4×4 matrix

$$[\underline{\underline{P}}_j]=\begin{bmatrix}0 & 0 & 0 & \omega\mu_0-\frac{\kappa^2}{\omega\epsilon_0\epsilon_{rj}}\\ 0 & 0 & -\omega\mu_0 & 0\\ 0 & -\omega\epsilon_0\epsilon_{rj}+\frac{\kappa^2}{\omega\mu_0} & 0 & 0\\ \omega\epsilon_0\epsilon_{rj} & 0 & 0 & 0\end{bmatrix},\qquad j\in[1,\infty). \tag{4}$$

The optical response of one period of the PMLID material is contained in the matrix

$$[\underline{\underline{Q}}]=\exp(i[\underline{\underline{P}}_N]d_N)\cdot\exp(i[\underline{\underline{P}}_{N-1}]d_{N-1})\cdot\ldots\cdot\exp(i[\underline{\underline{P}}_2]d_2)\cdot\exp(i[\underline{\underline{P}}_1]d_1) \tag{5}$$

for a specific value of κ. Let $[\mathbf{t}]^{(n)}$, $n\in[1,4]$, be the eigenvector corresponding to the nth eigenvalue σ_n of $[\underline{\underline{Q}}]$. After ensuring that $\mathrm{Re}[\ln(\sigma_{1,2})]<0$ [22], we set

$$[\mathbf{f}(0+)]=b_1[\mathbf{t}]^{(1)}+b_2[\mathbf{t}]^{(2)} \tag{6}$$

for SPP-wave propagation, where b_1 and b_2 are unknown dimensionless scalars. At the same time, $[\mathbf{f}(0-)]$ can be found in terms of a_p and a_s. Continuity of the tangential components of the electric and magnetic field phasors across the plane $z=0$ requires that $[\mathbf{f}(0-)]=[\mathbf{f}(0+)]$, which yields a dispersion equation for surface-wave propagation. This equation has to be solved in order to determine the SPP wavenumber κ.

B. Practical Boundary-Value Problem: Periodically Corrugated Metal/PMLID Interface

Let us now consider the boundary-value problem shown schematically in Fig. 2. This boundary-value problem is formulated using the rigorous coupled-wave analysis (RCWA) technique [23–26]. The regions $z < 0$ and $z > L_t = L_d + L_g + L_m$ are vacuous, the region $0 \le z \le L_d$ is occupied by the same PMLID material as in Subsection 2.A, with its relative permittivity $\epsilon_d(z)$ a piecewise uniform function of z, and the region $L_d + L_g \le z \le L_t$ by a metal of relative permittivity ϵ_m. The region $L_d < z < L_d + L_g$ contains a rectangular surface-relief grating of period L along the x axis and height L_g. With $0 < L_g < d_1$, the relative permittivity $\epsilon_g(x,z) = \epsilon_g(x \pm L, z)$ is described as

$$\epsilon_g(x,z) = \begin{cases} \epsilon_m, & x \in [0, L_1] \\ \epsilon_{r1}, & x \in [L_1, L] \end{cases}, \tag{7}$$

for $x \in [0, L]$ and $z \in (L_d, L_d + L_g)$. Let us note that the dimensions along the z axis are such that the ratio $N_p = L_d/2\Omega$ is an integer—the number of periods of the PMLID material.

In the vacuous half-space $z \le 0$, let a plane wave propagating in the x–z plane at an angle θ with respect to the z axis, be incident on the structure. Hence, the incident, reflected, and transmitted electric field phasors may be written in terms of Floquet harmonics as follows:

$$\mathbf{E}_{\rm inc}(\mathbf{r}) = \sum_{n\in\mathbb{Z}} (\hat{\mathbf{u}}_y a_s^{(n)} + \mathbf{p}_{+n} a_p^{(n)}) \exp[i(k_x^{(n)} x + k_z^{(n)} z)], \quad z \le 0, \tag{8}$$

$$\mathbf{E}_{\rm ref}(\mathbf{r}) = \sum_{n\in\mathbb{Z}} (\hat{\mathbf{u}}_y r_s^{(n)} + \mathbf{p}_{-n} r_p^{(n)}) \exp[i(k_x^{(n)} x - k_z^{(n)} z)], \quad z \le 0, \tag{9}$$

$$\mathbf{E}_{\rm tr}(\mathbf{r}) = \sum_{n\in\mathbb{Z}} (\hat{\mathbf{u}}_y t_s^{(n)} + \mathbf{p}_{+n} t_p^{(n)}) \exp\{i[k_x^{(n)} x + k_z^{(n)} (z - L_t)]\}, \quad z \ge L_t, \tag{10}$$

where

$$p_n^{\pm} = \mp \frac{k_z^{(n)}}{k_0} \hat{\mathbf{u}}_x + \frac{k_x^{(n)}}{k_0} \hat{\mathbf{u}}_z, \tag{11}$$

$k_x^{(n)} = k_0 \sin\theta + n\kappa_x$, $\kappa_x = 2\pi/L$, and

$$k_z^{(n)} = \begin{cases} +\sqrt{k_0^2 - (k_x^{(n)})^2}, & k_0^2 > (k_x^{(n)})^2 \\ +i\sqrt{(k_x^{(n)})^2 - k_0^2}, & k_0^2 < (k_x^{(n)})^2 \end{cases}. \tag{12}$$

The subscripts p and s represent the p- and s-polarization states, respectively. The incidence amplitudes $\{a_p^{(n)}, a_s^{(n)}\}_{n\in\mathbb{Z}}$ are presumably known. For plane-wave incidence, $a_p^{(n)} = a_s^{(n)} = 0 \forall\ n \ne 0$; furthermore, $a_p^{(0)} \ne 0$ and $a_s^{(0)} = 0$ for p-polarized incidence, and $a_p^{(0)} = 0$ and $a_s^{(0)} \ne 0$ for s-polarized incidence. The reflection amplitudes $\{r_p^{(n)}, r_s^{(n)}\}_{n\in\mathbb{Z}}$ and transmission amplitudes $\{t_p^{(n)}, t_s^{(n)}\}_{n\in\mathbb{Z}}$ have to be determined by solving a boundary-value problem.

The relative permittivity in the region $0 \le z \le L_t$ can be expanded as a Fourier series with respect to x, viz.,

$$\epsilon(x,z) = \sum_{n\in\mathbb{Z}} \epsilon^{(n)}(z) \exp(in\kappa_x x), \qquad z \in [0, L_t], \tag{13}$$

where

$$\epsilon^{(0)}(z) = \begin{cases} \epsilon_d(z), & z \in [0, L_d] \\ \frac{1}{L}\int_0^L \epsilon_g(x,z)\mathrm{d}x, & z \in (L_d, L_d + L_g], \\ \epsilon_m, & z \in [L_d + L_g, L_t] \end{cases} \tag{14}$$

$$\epsilon^{(n)}(z) = \begin{cases} \frac{1}{L}\int_0^L \epsilon_g(x,z)\exp(-in\kappa_x x)\mathrm{d}x, & z \in [L_d, L_d + L_g] \\ 0, & \text{otherwise} \end{cases}; \ \forall n \ne 0. \tag{15}$$

Since the right sides of Eqs. (8)–(10) and (13) contain infinite number of terms, RCWA requires restricting the index $n \in [-N_t, N_t]$, where N_t is large enough to deliver converged solutions. The solution algorithm to solve for unknown transmission and reflection amplitudes has been presented in detail elsewhere [19,23–28].

As the plane of incidence and the plane of the surface-relief grating are identical, depolarization does not occur. For p-polarized incidence, we set all incidence coefficients equal to zero, except $a_p^{(0)} = 1\ \mathrm{V\,m^{-1}}$, and compute the modal reflectances $R_p^{(n)} = |r_p^{(n)}|^2 \,\mathrm{Re}[k_z^{(n)}]/k_0 \cos\theta$ and modal transmittances $T_p^{(n)} = |t_p^{(n)}|^2 \,\mathrm{Re}[k_z^{(n)}]/k_0 \cos\theta$. For s-polarized incidence, we set all incidence coefficients equal to zero except $a_s^{(0)} = 1\ \mathrm{V\,m^{-1}}$ and compute the modal reflectances $R_s^{(n)} = |r_s^{(n)}|^2 \,\mathrm{Re}[k_z^{(n)}]/k_0 \cos\theta$ and modal transmittances $T_s^{(n)} = |t_s^{(n)}|^2 \mathrm{Re}[k_z^{(n)}]/k_0 \cos\theta$. Thus, the total reflectance, total transmittance, and absorptance are computed, respectively, as

$$R_p = \sum_{n=-N_t}^{N_t} R_p^{(n)}, \quad T_p = \sum_{n=-N_t}^{N_t} T_p^{(n)}, \quad A_p = 1 - R_p - T_p, \tag{16}$$

for p-polarized incidence; and

$$R_s = \sum_{n=-N_t}^{N_t} R_s^{(n)}, \quad T_s = \sum_{n=-N_t}^{N_t} T_s^{(n)}, \quad A_s = 1 - R_s - T_s, \tag{17}$$

for s-polarized incidence. For all numerical results reported in the following section, a sufficiently high value of N_t was chosen, as described in Subsection 3.C.

3. NUMERICAL RESULTS AND DISCUSSION

A. Experimental Data

In order to obtain realistic numerical results, the relative permittivities used for the metal and the dielectric layers in the calculations were obtained experimentally.

1. Metal

The metal was taken to be silver grown by evaporation. A silicon wafer was coated with 20 nm of chromium followed by 150 nm of silver using electron-beam evaporation. Silver was evaporated at a rate of $0.1\ \mathrm{nm\,s^{-1}}$ at a pressure of 8×10^{-7} Torr, while the substrate was held at ambient temperature. The silver film was characterized using

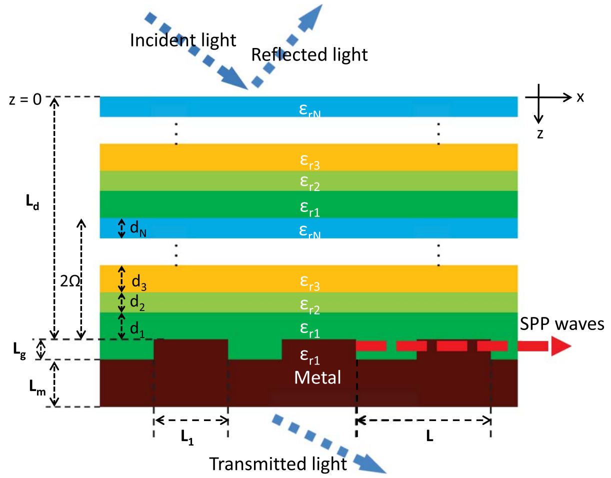

Fig. 2. (Color online) Schematic of the boundary-value problem involving a periodically corrugated interface between a homogeneous and isotropic metal and a periodic multilayered isotropic dielectric material.

spectroscopic ellipsometry [29] on a Woollam RC2 system. The measured real and imaginary parts of the ϵ_m are plotted in Fig. 3 as functions of λ_0.

2. Dielectric Materials

The PMLID material was taken to have $N = 9$ dielectric layers in its unit cell. Each of these dielectric materials was individually deposited on a microscopic glass slide and silicon wafers with bare native oxide, using plasma-enhanced chemical vapor deposition of a specific composition of silane, ammonia, and nitrous oxide in an Applied Materials P-5000 cluster tool. Each material was deposited as a 75-nm-thick film at a susceptor temperature of 300 °C, a pressure of 3.5 Torr, and RF plasma power of 300 W. Thus, each material has silicon oxide and silicon nitride in a particular ratio, as shown in Table 1, and may be classified as either silicon oxide or silicon nitride or a silicon oxynitride, all of the amorphous type.

Each dielectric material was characterized by spectroscopic ellipsometry on a Woollam RC2 system. Whereas the imaginary part of the relative permittivity of each material was found to be smaller than 10^{-4} for $\lambda_0 \in [400, 1100]$ nm, Cauchy coefficients for the real part were fitted to the experimental data to yield

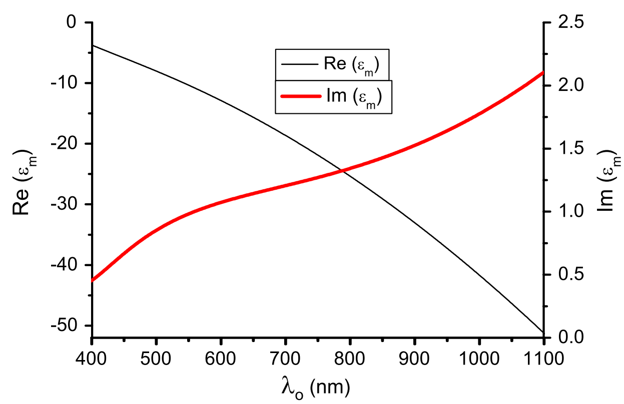

Fig. 3. (Color online) Measured values of the real and imaginary parts of the relative permittivity ϵ_m of evaporated silver with respect to the free-space wavelength λ_0. These data were used for the numerical results presented in Subsections 3.B and 3.C.

Table 1. Composition and Cauchy Coefficients for Nine Dielectric Layers in the PMLID Material[a]

Index j	SiO_2 %	SiN_x %	A_j	B_j (nm)^2	C_j (nm)^4
1	0	100	1.94	1.44×10^4	1.27×10^9
2	32	68	1.79	9.33×10^3	6.76×10^8
3	40	60	1.75	8.76×10^3	5.45×10^8
4	49	51	1.71	8.58×10^3	3.60×10^8
5	62	38	1.64	7.31×10^3	1.36×10^8
6	72	28	1.60	6.57×10^3	7.65×10^7
7	82	18	1.55	5.65×10^3	5.65×10^7
8	90	10	1.51	4.63×10^3	5.01×10^7
9	100	0	1.47	2.95×10^3	6.10×10^7

[a]Spectra of the real parts of the relative permittivity of the dielectric layers are plotted in Fig. 4.

$$\mathrm{Re}(\epsilon_{rj}) = \left(A_j + \frac{B_j}{\lambda_0^2} + \frac{C_j}{\lambda_0^4}\right)^2, \qquad j \in [1, 9]. \tag{18}$$

The chemical composition and the Cauchy coefficients are provided in Table 1, and the plots of $\mathrm{Re}(\varepsilon_{rj})$, $j \in [1, 9]$, with respect to λ_0 in Fig. 4.

B. Solutions of the Canonical Boundary-Value Problem

A Mathematica program was written and implemented to solve the dispersion equation mentioned in Subsection 2.A, using a sequential combination of the search and the Newton–Raphson methods [30] for $\lambda_0 \in [400, 1100]$ nm. The metal was taken to be evaporated silver with relative permittivity given in Fig. 3. Each unit cell of the PMLID material was supposed to have $N = 9$ layers, each of thickness 75 nm, with relative permittivities given in Fig. 4.

The relative phase speed $v_p/c = k_0/\mathrm{Re}(\kappa)$ and the e-folding distance $\Delta_x = 1/\mathrm{Im}(\kappa)$ along the direction of propagation are plotted in Fig. 5 for each solution of the dispersion equation that we found. The solutions are organized in six branches: $p1$, $p2$, and $p3$ for p-polarized SPP waves; and $s1$, $s2$, and $s3$ for s-polarized SPP waves. Thus, multiple SPP waves of both p- and s-polarization states can be guided by the planar metal/PMLID interface. The number of SPP waves depends on the free-space wavelength λ_0. More accurately, it depends on the *reduced period* $2\Omega/\lambda_0$ of the PMLID material.

Figure 5 shows another branch, labeled $p0$. It is not a solution of the metal/PMLID problem. Instead, it is a solution of the canonical problem when the PMLID material is entirely replaced by a homogeneous dielectric material of relative permittivity ϵ_{r1}—the relative permittivity of the layer of the PMLID material that is adjacent to the metal. The wavenumber for the $p0$ branch is given by [31]

$$\kappa_{p0} = k_0 \sqrt{\frac{\epsilon_m \epsilon_{r1}}{\epsilon_m + \epsilon_{r1}}}. \tag{19}$$

For $\lambda_0 < 540$ nm, the $p0$ branch coincides with the $p1$ branch, indicating that the SPP wave guided by the metal/PMLID interface diminishes so rapidly in the PMLID half-space that its magnitudes in the second and later layers of the PMLID material are vanishingly small. That was also the reason that the computer program implemented to solve the dispersion equation of Subsection 2.A could not converge for the $p1$ branch when $\lambda_0 < 526$ nm. However, when λ_0 increases above

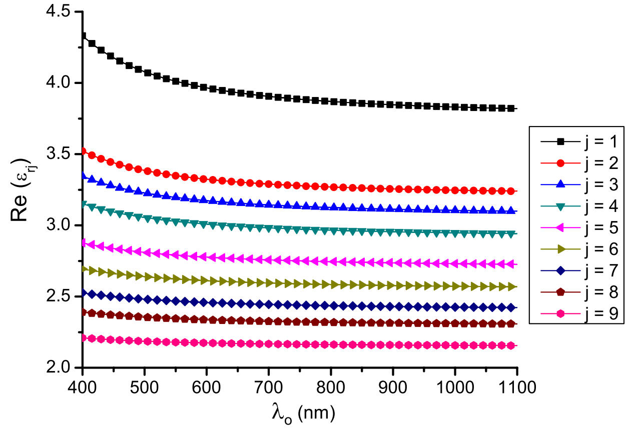

Fig. 4. (Color online) Measured values of the real parts of relative permittivity ϵ_{rj} of nine dielectric materials (used to make the PMLID material) with respect to the free-space wavelength λ_0. The imaginary parts are all less than 10^{-4} and were therefore ignored. These data were used for the numerical results presented in Subsections 3.B and 3.C. The composition and the Cauchy coefficients of the dielectric layers are given in Table 1.

540 nm, the branch $p1$ is not the same as $p0$, and the computer program worked well. All other branches (i.e., $p2$, $p3$, and $s1$–$s3$) represent the SPP waves that have spatial extent beyond the first layer for $\lambda_0 \in [400, 1100]$ nm; therefore, those solutions of the dispersion equation were found without difficulty.

Parenthetically, we note here that all solutions of the dispersion equation of Subsection 2.A may not have been found by our algorithm to solve it, because of the nonlinear nature of the dispersion equation. Therefore, the solutions of the dispersion equation presented in Fig. 5 should not be considered the complete set of solutions.

C. Results for the Practical Boundary-Value Problem

Let us now proceed toward the numerical results for the main work reported in this paper: the excitation of multiple SPP waves in the grating-coupled configuration described in Subsection 2.B. Both the metal and the PMLID material were taken to be the same as in Subsection 3.B. Moreover, we chose $L_1 = 0.5L$, $L = 400$ nm, $L_g = 35$ nm, and $L_m = 30$ nm for representative results. The number of terms in Eqs. (8)–(10) and (13) was restricted to 25 (i.e., $N_t = 12$) in our computer program after ascertaining that all nonzero modal reflectances and the absorptances converged to within 1% of their value for $N_t = 11$. Since $N = 9$ and $d_j = 75$ nm $\forall j \in [1, 9]$, $\Omega = 337.5$ nm. The number N_p of periods was kept variable. For illustrative purposes, the results for $\lambda_0 = 500$ nm and $\lambda_0 = 700$ nm are presented in this section.

1. $\lambda_0 = 500$ nm

The relative wavenumbers κ/k_0 that satisfy the dispersion equation of the canonical boundary-value problem for $\lambda_0 = 500$ nm are provided in Table 2. To study the excitation of these SPP waves in the grating-coupled configuration, the total reflectances R_p and R_s were calculated as functions of the incidence angle θ and are presented in Figs. 6(a) and 6(c), respectively, for three values of N_p: 1, 2, and 3. The dips in the these plots that are independent of the value of N_p may represent the excitation of SPP waves and are highlighted by vertical arrows in Figs. 6(a) and 6(c). However, it is possible that the reflectance dips are caused by the increase in transmittance and could be false indication of the excitation of SPP waves. Therefore, to have an unequivocal proof that the decrease in reflectance indicates the excitation of SPP waves, the absorptances A_p and A_s were also calculated as functions of θ and are presented in Figs. 6(b) and 6(d), respectively, when $N_p = 1$, 2, and 3.

In Fig. 6(b), three A_p peaks are identified by vertical arrows. The peaks are located at $\theta \simeq 14.5°$, 26.2°, and 55.2° when $N_p = 3$, but at slightly different values of θ for the lower values of N_p. We have ensured that the locations of these peaks do not change significantly for N_p as high as 6. These peaks represent the excitation of p-polarized SPP waves [19,28]. The locations of other peaks in Fig. 6(b) are dependent on the value of N_p, and, therefore, represent the excitation of waveguide modes [32,33] whose characteristics depend on the thickness of the PMLID material. The relative wavenumbers of several Floquet harmonics at the θ values of the identified

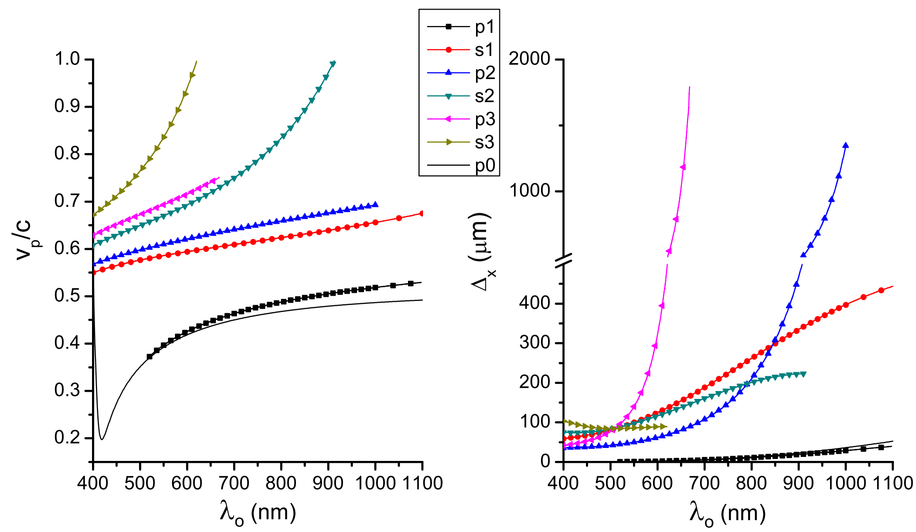

Fig. 5. (Color online) Left, relative phase speed v_p/c and, right, e-folding distance Δ_x of possible SPP waves guided by the planar metal/PMLID interface. The relative wavenumbers κ/k_0 were obtained by the solution of the canonical boundary-value problem described in Subsection 2.A, except for the black solid curve (labeled $p0$) that was obtained by the solution of Eq. (19).

Table 2. Relative Wavenumbers κ/k_0 of Possible SPP Waves for $\lambda_0 = 500$ nm Obtained by the Solution of the Canonical Boundary-Value Problem Described in Subsection 2.A, Except for the Italicized Entry that was Obtained by the Solution of Eq. (19)[a]

p-pol	$2.8470 + 0.1506i$	$1.6716 + 0.0019i$	$1.4866 + 0.0010i$
s-pol	$1.7336 + 0.0010i$	$1.5389 + 0.0010i$	$1.3066 + 0.0009i$

[a] If κ represents an SPP wave propagating coparallel to $\hat{\mathbf{u}}_x$, $-\kappa$ represents an SPP wave propagating antiparallel to $\hat{\mathbf{u}}_x$.

peaks are given in Table 3. A comparison of Tables 2 and 3 shows that, at $\theta = 14.5°$, $k_x^{(1)}/k_0 = 1.5004$ is very close to $\mathrm{Re}(1.4866 + 0.0010i)$; likewise, at $\theta = 26.2°$, $k_x^{(1)}/k_0 = 1.6915$ is very close to $\mathrm{Re}(1.6716 + 0.0019i)$. Therefore, these two A_p peaks represent the excitation of p-polarized SPP waves as Floquet harmonics of order $n = 1$. This conclusion is reinforced by the spatial profile of the x-component P_x of the time-averaged Poynting vector,

$$\mathbf{P}(x,z) = \frac{1}{2}\,\mathrm{Re}[\mathbf{E}(x,z) \times \mathbf{H}^*(x,z)], \tag{20}$$

presented in Fig. 7 along the line ($x = 0.75L$, $y = 0$) normal to the mean metal/PMLID plane when $N_p = 3$. The figure shows that, at $\theta = 14.5°$ and $26.2°$, two surface waves are being guided by the metal/PMLID grating; however, the SPP wave excited at $\theta = 26.2°$ is more localized than the one excited at $\theta = 14.5°$. Moreover, both the SPP waves are propagating coparallel with $\hat{\mathbf{u}}_x$.

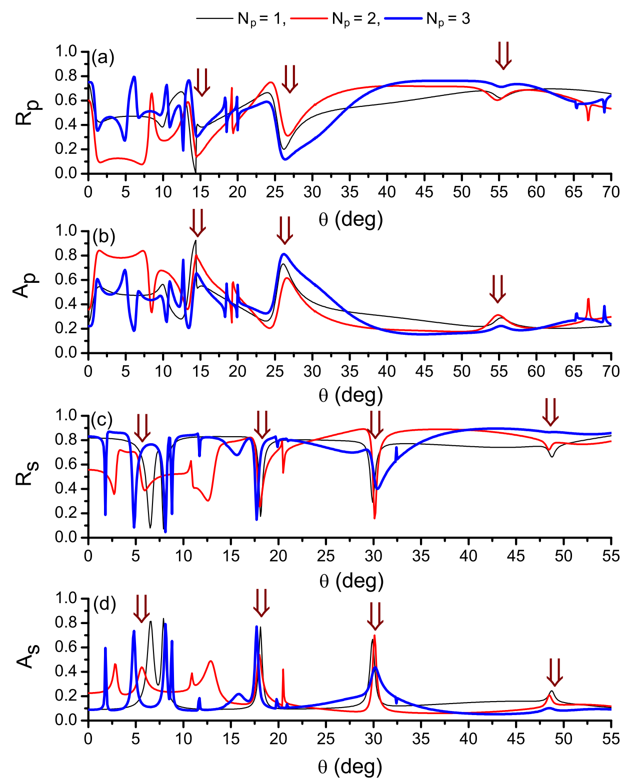

Fig. 6. (Color online) Total reflectances (a) R_p and (c) R_s, and absorptances (b) A_p and (d) A_s versus the angle of incidence θ when $\lambda_0 = 500$ nm, $L = 400$ nm, $L_1 = 0.5L$, $L_g = 35$ nm, $L_m = 30$ nm, and $L_d = 2\Omega N_p$. The vertical arrows identify the reflectance dips or absorptance peaks that represent the excitation of SPP waves.

Table 3. Relative Wavenumbers $k_x^{(n)}/k_0$ of Floquet Harmonics at the θ-Values of the Peaks Identified by Vertical Arrows in Fig. 6 when $\lambda_0 = 500$ nm, $N_p = 3$, and $L = 400$ nm[a]

	$n = -2$	$n = -1$	$n = 0$	$n = 1$	$n = 2$
$\theta = 4.8°$	−2.4163	−1.16632	0.0837	**1.3337**	2.5837
$\theta = 14.5°$	−2.2496	−0.9996	0.2504	**1.5004**	2.7504
$\theta = 17.7°$	−2.1960	−0.9460	0.3040	**1.5540**	2.8040
$\theta = 26.2°$	−2.0585	−0.8085	0.4415	**1.6915**	2.9415
$\theta = 30.2°$	−1.9970	−0.7470	0.5030	**1.7530**	3.0030
$\theta = 48.5°$	**−1.7510**	−0.5010	0.7490	1.9990	3.2490
$\theta = 55.2°$	−1.6788	−0.4288	0.8212	2.0712	**3.3212**

[a] Boldface entries signify SPP waves.

The peak at $\theta = 55.2°$ in Fig. 6(b) also represents a p-polarized SPP wave as a Floquet harmonic of positive order, as can be seen by the spatial profile of P_x given also in Fig. 7, because the SPP wave is propagating along $\hat{\mathbf{u}}_x$. The very low magnitude of A_p at the peak and the subsequent low intensity of P_x in Fig. 7 support the inference that this p-polarized SPP wave is excited as a Floquet harmonic of order $n = 2$ because it has been shown elsewhere [19,34,35] that the SPP waves that are excited as a Floquet harmonic of second order tend to have lower absorptance peaks. The spatial profile also shows that this p-polarized SPP wave is tightly localized to the metal/PMLID grating. Now, at $\theta = 55.2°$, $k_x^{(2)}/k_0 = 3.3212$ in Table 3. But a corresponding solution on the $p1$ branch could not be delivered by our computer program, as discussed in Subsection 3.B. Although Eq. (19) did deliver $\kappa/k_0 = 2.8470 + 0.1506i$ on the $p0$ branch, its real part is not close to $k_x^{(2)}/k_0 = 3.3212$ in Table 3. We conjecture that this A_p peak does represent the excitation of a p-polarized SPP wave, the significant difference between $k_x^{(2)}/k_0 = 3.3212$ and $\mathrm{Re}(2.8470 + 0.1506i)$ being due to the fact that the SPP wave is tightly bound to the metal/PMLID interface in the canonical boundary-value problem. Since $\kappa/k_0 = 2.8470 + 0.1506i$ was obtained assuming the metal/PMLID interface to be planar and $k_x^{(2)}/k_0 = 3.3212$ is for an SPP wave guided by the metal/PMLID grating, we think the surface roughness has a hugely significant effect on the relative wavenumber of the SPP wave due to its very strong localization to the metal/PMLID interface.

In the plots of A_s versus θ in Fig. 6(d), four peaks represent the excitation of s-polarized SPP waves: $\theta \simeq 4.8°$, $17.7°$, $30.2°$, and $48.5°$ (for $N_p = 3$). The relative wavenumbers of several Floquet harmonics at these values of θ are provided in Table 3. A comparison of Tables 2 and 3 shows that (i) at $\theta = 4.8°$, $k_x^{(1)}/k_0 = 1.3337$ is very close to $\mathrm{Re}(1.3066 + 0.0009i)$, and (ii) at $\theta = 17.7°$, $k_x^{(1)}/k_0 = 1.5540$ is very close to $\mathrm{Re}(1.5389 + 0.0010i)$. Therefore, these two A_s peaks represent the excitation of s-polarized SPP waves as a Floquet harmonic of order $n = 1$. The spatial variations of P_x at these values of θ in Fig. 8 also support this conclusion. Moreover, both of these s-polarized SPP waves are loosely localized to the metal/PMLID interface in the PMLID material, with the s-polarized SPP wave excited at $\theta = 4.8°$ having more spatial extension into the PMLID material than the SPP wave at excited at $\theta = 17.7°$. The spatial extensions of these two SPP waves in the PMLID material explain the apparent dependence of these A_s peaks on N_p. However, we have verified that the locations of these peaks are independent of N_p for $N_p > 6$.

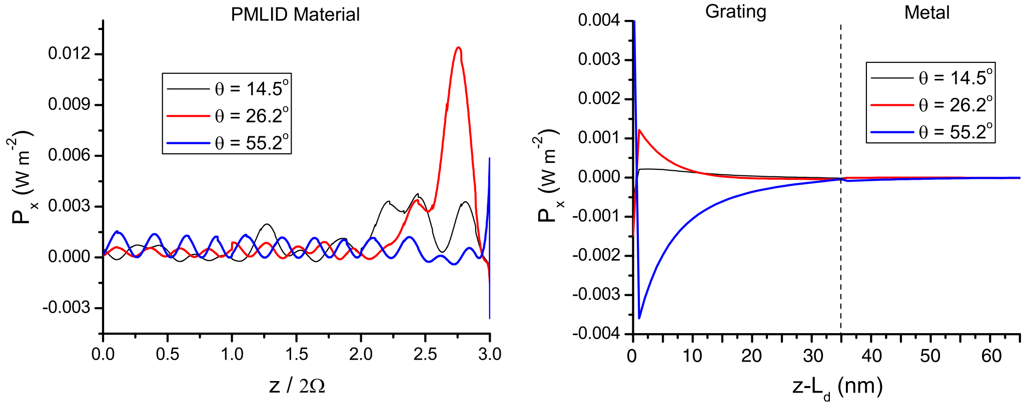

Fig. 7. (Color online) Variation of the x-component $P_x(x,z)$ of the time-averaged Poynting vector $\mathbf{P}(x,z)$ along the z axis in the regions (left) $0 < z < L_d$ and (right) $L_d < z < L_d + L_g + L_m$, when $\lambda_0 = 500$ nm, $x = 0.75L$, $N_p = 3$, $L_g = 35$ nm, $L_m = 30$ nm, and $L = 400$ nm. The incident plane wave is p polarized with $a_p^{(0)} = 1\ \mathrm{V\,m^{-1}}$, and the angles of incidence are those of the peaks identified by vertical arrows in Fig. 6(b).

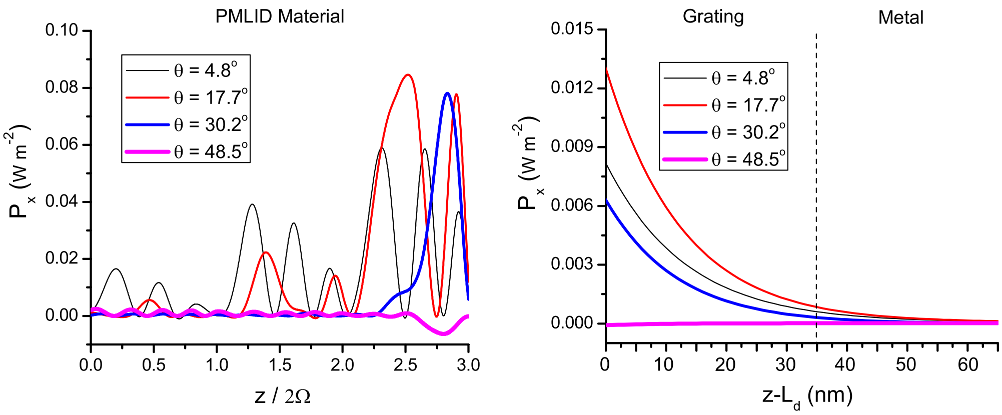

Fig. 8. (Color online) Same as Fig. 7, except that the incident plane wave is s polarized with $a_s^{(0)} = 1\ \mathrm{V\,m^{-1}}$, and the angles of incidence are those of the peaks identified by vertical arrows in Fig. 6(d).

At $\theta = 30.2°$ and $48.5°$ in Fig. 6(d), the same s-polarized SPP wave is excited; however, it is excited as a Floquet harmonic of order $n = 1$ at $\theta = 30.2°$ because $k_x^{(1)}/k_0 = 1.7530$ is very close to $\mathrm{Re}(1.7336 + 0.0010i)$ and as a Floquet harmonic of order $n = -2$ at $\theta = 48.5°$ as $k_x^{(-2)}/k_0 = -1.7510$ is very close to $\mathrm{Re}(-1.7336 - 0.0010i)$. This is also evident from the spatial profiles in Fig. 8 because, at $\theta = 30.2°$, the s-polarized SPP wave is propagating along $\hat{\mathbf{u}}_x$, whereas, at $\theta = 48.5°$, the same SPP wave is propagating along $-\hat{\mathbf{u}}_x$.

Let us note that, in Fig. 6(c), the reflectance does not decrease at $\theta = 48.5°$ (even though an s-polarized SPP wave is excited at this angle) when $N_p = 3$. However, the absorptance peak in Fig. 6(d) at the same value of θ when $N_p = 3$ indicates that, instead of a decrease in the reflectance, the transmittance has decreased. So, the reflectance plots do not always possess complete information and should be used carefully in analyses for SPP-wave excitation.

Table 4. Same as Table 2, Except for $\lambda_0 = 700$ nm

p-pol	$2.1572 + 0.0208i$	$1.5592 + 0.0010i$
s-pol	$1.6401 + 0.0006i$	$1.3322 + 0.0007i$

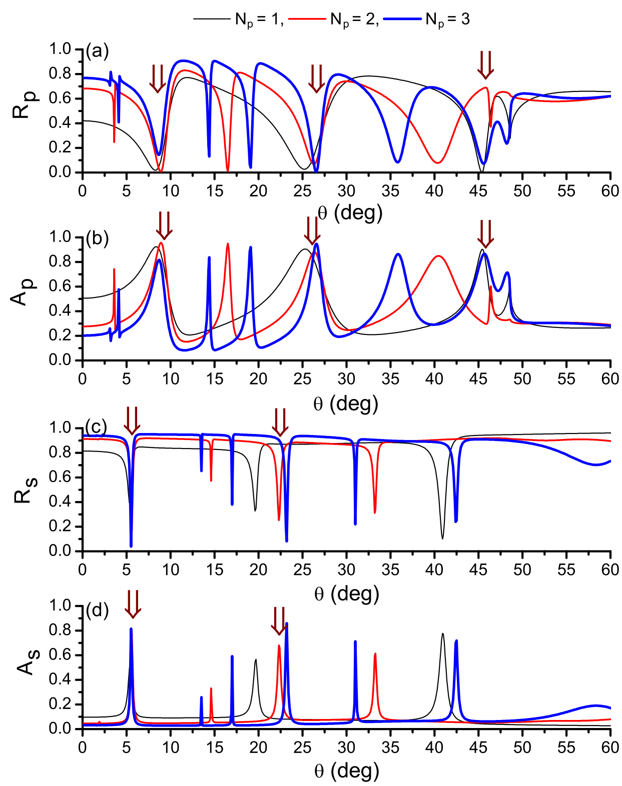

Fig. 9. (Color online) Same as Fig. 6, except for $\lambda_0 = 700$ nm.

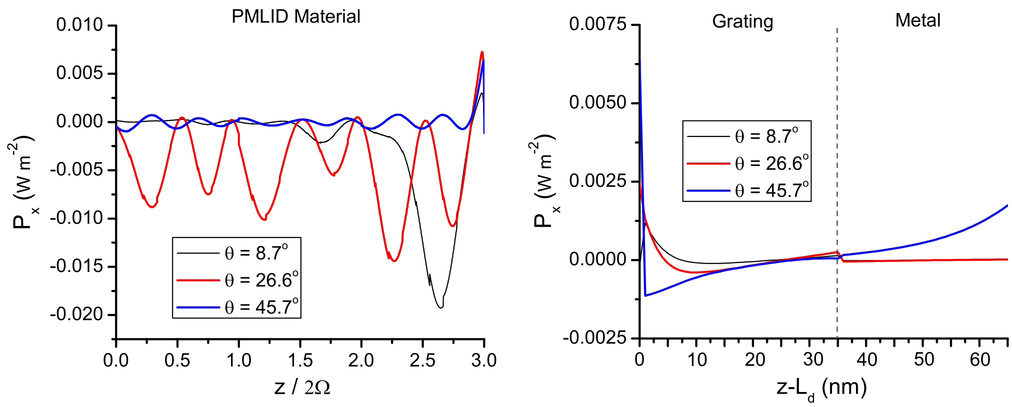

Fig. 10. (Color online) Same as Fig. 7, except that $\lambda_0 = 700$ nm and the angles of incidence are those of the peaks identified by vertical arrows in Fig. 9(b).

2. $\lambda_0 = 700$ nm

The relative wavenumbers κ/k_0 that satisfy the dispersion equation of the canonical boundary-value problem for $\lambda_0 = 700$ nm are provided in Table 4. The table shows that at least two p- and two s-polarized SPP waves can be guided by the planar metal/PMLID interface.

Plots of the total reflectances and absorptances versus θ are presented in Fig. 9 when $N_p = 1$, 2, and 3. In the plots of A_p in Fig. 9(b), three peaks are present, independent of the value of N_p: $\theta \simeq 8.7°$, 26.6°, and 45.7°. The relative wavenumbers of several Floquet harmonics at these values of θ are provided in Table 5. At $\theta = 8.7°$, $k_x^{(-1)}/k_0 = -1.5987$ in Table 5 is very close to $\mathrm{Re}(-1.5592 - 0.0010i)$ in Table 4; therefore, this peak represents the excitation of a p-polarized SPP wave as a Floquet harmonic of order $n = -1$. The spatial profile of P_x given in Fig. 10 for $\theta = 8.7°$ also supports this conclusion, with the SPP wave propagating antiparallel to $\hat{\mathbf{u}}_x$.

At $\theta = 45.7°$ in Fig. 9(b), the A_p peak represents the excitation of another p-polarized SPP wave as a Floquet harmonic of order $n = 1$ because $k_x^{(1)}/k_0 = 2.4657$ in Table 5 is close to $\mathrm{Re}(2.1572 + 0.0208i)$ in Table 4. The agreement between $k_x^{(1)}/k_0 = 2.4657$ and $\mathrm{Re}(2.1572 + 0.0208i)$ is not very strong, due to the high localization of the SPP wave to the metal/PMLID interface, as can be ascertained from the spatial profile presented in Fig. 10 for $\theta = 45.7°$.

At $\theta = 26.6°$ in Fig. 9(b), the A_p peak is independent of N_p and the spatial profile of P_x given in Fig. 10 also shows that a surface wave is propagating along $-\hat{\mathbf{u}}_x$. However, $k_x^{(-1)}/k_0 = -1.3022$ in Table 5 is not close to the real part of any of the solutions for p-polarized SPP waves given in Table 4. The plots (not shown) of the real and imaginary parts of the solution of the dispersion equation of Subsection 2.A versus $\mathrm{Re}(\kappa)$ around $\kappa = 1.3k_0$ showed that a solution does exist near this value of κ, but the slopes of the plots are so high that the solution algorithm was unable to converge to the solution. So, we conjecture that the A_p peak at $\theta = 26.6°$ does represent the excitation of a p-polarized SPP wave.

In the plots of A_s versus θ in Fig. 9(d), s-polarized SPP waves are excited at two values of θ: 5.4° and 23.2°. The relative wavenumbers of several Floquet harmonics at these values of θ are given in Table 5. A comparison of Tables 4 and 5 shows that, at $\theta = 5.4°$, $k_x^{(-1)}/k_0 = -1.6559$ is very close to $\mathrm{Re}(-1.6401 - 0.0006i)$. Similarly, at $\theta = 23.2°$, $k_x^{(-1)}/k_0 = -1.3561$ is very close to $\mathrm{Re}(-1.3322 - 0.0007i)$. Therefore, these two A_s peaks represent the excitation of s-polarized SPP waves as Floquet harmonics of order $n = -1$. The spatial variations of P_x in Fig. 11 also support this conclusion as both SPP waves are propagating along $-\hat{\mathbf{u}}_x$.

However, the s-polarized SPP wave excited at $\theta \simeq 23.2°$ is loosely bound to the metal/PMLID grating. This is also reflected in the slight shift in the θ value of the A_s peak in Fig. 9(d) when N_p changes from 1 to 3. However, the difference between the θ positions of the peak when $N_p = 2$ and $N_p = 3$ is less than the difference between the θ positions when $N_p = 1$ and $N_p = 2$; and, for sufficiently high value of N_p, we have computationally determined that the A_s peak at $\theta \simeq 23.2°$ is independent of the value of N_p.

To demonstrate that the absorptance peaks that are not identified by vertical arrows represent the excitation of waveguide modes, we have presented the spatial variations of P_x in Fig. 12 when $\lambda_0 = 700$, the incident plane wave is s polarized, $N_p = 3$, and $\theta \in \{17°, 42.5°\}$. The two chosen values of θ are of the two peaks in Fig. 9(d) that do not represent the excitation of SPP waves. The spatial profiles in Fig. 12 show that the energy of either of these two guided waves is not localized to the metal/PMLID interface but is distributed in the bulk of the PMLID material. The spatial profiles (not shown) for other absorptance peaks that are not identified by vertical arrows show the same feature. Moreover,

(i) these peaks are present for some values of N_p but not for others, and

(ii) none of the relative wavenumbers of Floquet harmonics at these values of θ are close to the real parts of any of the relative wavenumbers of SPP waves obtained by the solution of the canonical boundary-value problem.

Table 5. Relative Wavenumbers $k_x^{(n)}/k_0$ of Floquet Harmonics at the θ-Values of the Peaks Identified in Fig. 9 when $\lambda_0 = 700$ nm, $N_p = 3$, and $L = 400$ nm[a]

	$n = -2$	$n = -1$	$n = 0$	$n = 1$	$n = 2$
$\theta = 5.4°$	−3.4059	**−1.6559**	0.0941	1.8441	3.5941
$\theta = 8.7°$	−3.3487	**−1.5987**	0.1513	1.9013	3.6513
$\theta = 23.2°$	−3.1061	**−1.3561**	0.3939	2.1439	3.8939
$\theta = 26.6°$	−3.0522	**−1.3022**	0.4478	2.1978	3.9478
$\theta = 45.7°$	−2.7843	−1.0343	0.7157	**2.4657**	4.2157

[a]Boldface entries signify SPP waves.

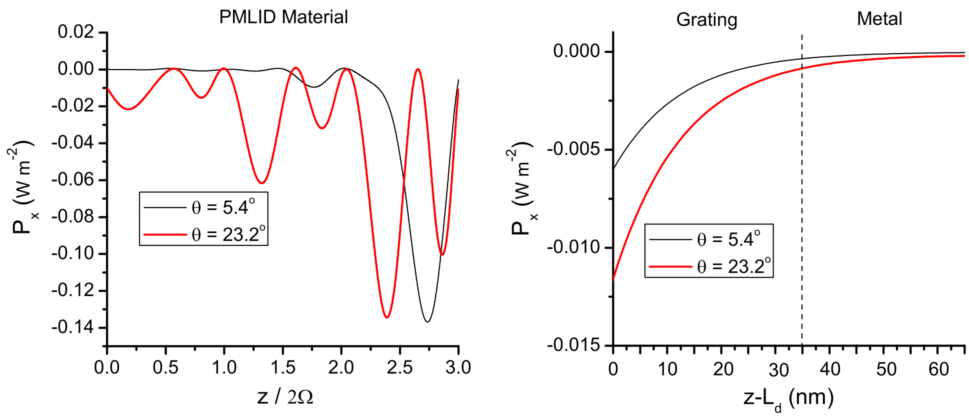

Fig. 11. (Color online) Same as Fig. 8, except that $\lambda_0 = 700$ nm and the angles of incidence are those of the peaks identified by vertical arrows in Fig. 9(d).

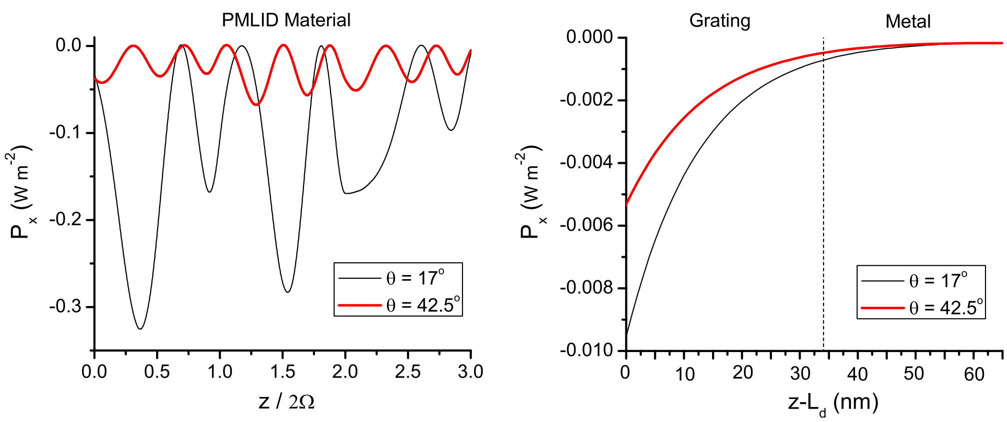

Fig. 12. (Color online) Same as Fig. 8, except that $\lambda_0 = 700$ nm and the angles of incidence are of the two chosen peaks in Fig. 9(d) that represent the excitation of waveguide modes.

4. CONCLUDING REMARKS

We formulated a boundary-value problem for the excitation of SPP waves by the periodically corrugated interface of a metal of finite thickness and a PMLID material with a finite number of periods. On this structure, a linearly polarized plane wave was taken to be obliquely incident, the plane of incidence being the same as the plane of corrugations. Using a numerically stable algorithm based on the well-known technique of RCWA, we solved the boundary-value problem and calculated the amplitudes of the Floquet harmonics in the reflected and the transmitted fields. The refractive indices of all materials were experimentally determined. Furthermore, with eventual application to thin-film solar cells in view, we ensured that the geometric parameters employed for the calculations are experimentally realizable.

For both p- and s-polarized incident plane waves, we examined the total reflectance and the absorptance of the structure as functions of the angle of incidence. Absorptance peaks independent of the number of periods of the PMLID material, when that material is sufficiently thick, indicated the excitation of SPP waves. These absorptance peaks were also correlated with the results of an underlying canonical boundary-value problem wherein solutions of a dispersion equation for the guidance of SPP waves by the planar interface of the metal and the PMLID material were obtained. That multiple SPP waves were obtained at any $\lambda_0 \in [400, 1100]$ nm, some with e-folding distances (along the direction of propagation) exceeding 100 μm, is promising for application in thin-film solar cells. The excitation of waveguide modes, in addition to SPP waves, will also play an important role in the enhancement of absorption in that application [28,36].

ACKNOWLEDGMENTS

We thank Nikolas Podraza (University of Toledo), Michael Motyka (Penn State), and David St. John (Penn State) for helpful discussions on spectroscopic ellipsometry. Discussions with Peter Monk (University of Delaware) and Theresa Mayer (Penn State) are also gratefully acknowledged. M. Faryad thanks SPIE for a research scholarship. Partial support for this work was provided by the U.S. National Science Foundation via grant No. DMR-1125591.

REFERENCES AND NOTES

1. P. Yeh, A. Yariv, and C.-S. Hong, “Electromagnetic propagation in periodic stratified media. I. General theory,” J. Opt. Soc. Am. **67**, 423–438 (1977).
2. J. A. Gaspar-Armenta and F. Villa, “Photonic surface-wave excitation: photonic crystal-metal interface,” J. Opt. Soc. Am. B **20**, 2349–2354 (2003).

3. W. M. Robertson and M. S. May, “Surface electromagnetic wave excitation on one-dimensional photonic band-gap arrays,” Appl. Phys. Lett. **74**, 1800–1802 (1999).
4. Z. Salamon, H. A. Macleod, and G. Tollin, “Coupled plasmon-waveguide resonators: a new spectroscopic tool for probing proteolipid film structure and properties,” Biophys. J. **73**, 2791–2797 (1997).
5. Z. Salamon and G. Tollin, “Optical anisotropy in lipid bilayer membrane: coupled plasmon-waveguide resonance measurements of molecular orientation, polarizability, and shape,” Biophys. J. **80**, 1557–1567 (2001).
6. M. Faryad and A. Lakhtakia, “On surface plasmon-polariton waves guided by the interface of a metal and a rugate filter with sinusoidal refractive-index profile,” J. Opt. Soc. Am. B **27**, 2218–2223 (2010).
7. M. Faryad and A. Lakhtakia, “On multiple surface-plasmon-polariton waves guided by the interface of a metal film and a rugate filter in the Kretschmann configuration,” Opt. Commun. **284**, 5678–5687 (2011).
8. B. G. Bovard, “Rugate filter theory: an overview,” Appl. Opt. **32**, 5427–5442 (1993).
9. P. W. Baumeister, *Optical Coating Technology* (SPIE, 2004), Sec. 5.3.3.2.
10. V. E. Ferry, M. A. Verschuuren, H. B. T. Li, E. Verhagen, R. J. Walters, R. E. I. Schropp, H. A. Atwater, and A. Polson, “Light trapping in ultrathin plasmonic solar cells,” Opt. Express **18**, A237–A245 (2010).
11. Y. Lu, J. F. Sell, M. D. Johnson, K. Reinhardt, and R. J. Knize, “Adding a thin metallic plasmonic layer to silicon thin film solar cells,” Phys. Status Solidi C **8**, 843–845 (2011).
12. Turbadar in 1959 [13] had anticipated the 1968 papers of both Otto [14] and Kretschmann and Raether [15], but had not used the word *plasmon*.
13. T. Turbadar, “Complete absorption of light by thin metal films,” Proc. Phys. Soc. London **73**, 40–44 (1959).
14. A. Otto, “Excitation of nonradiative surface plasma waves in silver by the method of frustrated total reflection,” Z. Phys. **216**, 398–410 (1968).
15. E. Kretschmann and H. Raether, “Radiative decay of non-radiative surface plasmons excited by light,” Z. Naturforsch. A **23**, 2135–2136 (1968).
16. V. N. Konopsky and E. V. Alieva, “Long-range propagation of plasmon polaritons in a thin metal film on a one-dimensional photonic crystal surface,” Phys. Rev. Lett. **97**, 253904 (2006).
17. J. Moreland, A. Adams, and P. K. Hansma, “Efficiency of light emission from surface plasmons,” Phys. Rev. B **25**, 2297–2300 (1982).
18. P. T. Worthing and W. L. Barnes, “Efficient coupling of surface plasmon polaritons to radiation using a bi-grating,” Appl. Phys. Lett. **79**, 3035–3037 (2001).
19. M. Faryad and A. Lakhtakia, “Grating-coupled excitation of multiple surface plasmon-polariton waves,” Phys. Rev. A **84**, 033852 (2011).
20. P. Sheng, A. N. Bloch, and R. S. Stepleman, “Wavelength-selective absorption enhancement in thin-film solar cells,” Appl. Phys. Lett. **43**, 579–581 (1983).
21. C. Heine and R. H. Morf, “Submicrometer gratings for solar energy applications,” Appl. Opt. **34**, 2476–2482 (1995).
22. A. Lakhtakia, “Reflection from a semi-infinite rugate filter,” J. Mod. Opt. **58**, 562–565 (2011).
23. L. Li, “Multilayer modal method for diffraction gratings of arbitrary profile, depth, and permittivity,” J. Opt. Soc. Am. A **10**, 2581–2591 (1993).
24. M. G. Moharam and T. K. Gaylord, “Diffraction analysis of dielectric surface-relief gratings,” J. Opt. Soc. Am. **72**, 1385–1392 (1982).
25. N. Chateau and J.-P. Hugonin, “Algorithm for the rigorous coupled-wave analysis of grating diffraction,” J. Opt. Soc. Am. A **11**, 1321–1331 (1994).
26. M. G. Moharam, E. B. Grann, and D. A. Pommet, “Formulation for stable and efficient implementation of the rigorous coupled-wave analysis of binary gratings,” J. Opt. Soc. Am. A **12**, 1068–1076 (1995).
27. F. Wang, M. W. Horn, and A. Lakhtakia, “Rigorous electromagnetic modeling of near-field phase-shifting contact lithography,” Microelectron. Eng. **71**, 34–53 (2004).
28. M. Faryad and A. Lakhtakia, “Enhanced absorption of light due to multiple surface-plasmon-polariton waves,” Proc. SPIE **8110**, 81100F (2011).
29. H. Fujiwara, *Spectroscopic Ellipsometry, Principles and Applications* (Wiley, 2007), pp. 82 and 190.
30. Y. Jaluria, *Computer Methods for Engineering* (Taylor & Francis, 1996).
31. J. Homola, ed., *Surface Plasmon Resonance Based Sensors* (Springer, 2006).
32. N. S. Kapany and J. J. Burke, *Optical Waveguides* (Academic, 1972).
33. D. Marcuse, *Theory of Dielectric Optical Waveguides* (Academic, 1991).
34. M. Faryad and A. Lakhtakia, “Multiple trains of same-color surface plasmon-polaritons guided by the planar interface of a metal and a sculptured nematic thin film. Part V: Grating-coupled excitation,” J. Nanophoton. **5**, 053527 (2011).
35. S. A. Maier, *Plasmonics: Fundamentals and Applications* (Springer, 2007).
36. T. Khaleque, J. Yoon, W. Wu, M. Shokooh-Saremi, and R. Magnusson, “Guided-mode-resonance enabled absorption in amorphous silicon for thin-film solar cell applications,” in *Integrated Photonics Research, Silicon and Nanophotonics*, OSA Technical Digest (CD) (Optical Society of America, 2011), paper ITuD3.